



OPEN ACCESS

EDITED BY

Wen Zhuang,
Shandong University, China

REVIEWED BY

Xueyan Jiang,
Ocean University of China, China
Deli Wang,
Xiamen University, China

Liqin Duan,
Institute of Oceanology Chinese Academy
of Sciences, China

*CORRESPONDENCE

Li Li

✉ Li.Li@fio.org.cn

RECEIVED 30 January 2023

ACCEPTED 18 May 2023

PUBLISHED 02 June 2023

CITATION

Wang X, Li L, Ren Y, Cao P, Zhu A, Liu J
and Shi X (2023) Early diagenesis and
benthic fluxes of redox-sensitive metals in
eastern China shelf sediments.
Front. Mar. Sci. 10:1154248.
doi: 10.3389/fmars.2023.1154248

COPYRIGHT

© 2023 Wang, Li, Ren, Cao, Zhu, Liu and Shi.
This is an open-access article distributed
under the terms of the [Creative Commons
Attribution License \(CC BY\)](https://creativecommons.org/licenses/by/4.0/). The use,
distribution or reproduction in other
forums is permitted, provided the original
author(s) and the copyright owner(s) are
credited and that the original publication in
this journal is cited, in accordance with
accepted academic practice. No use,
distribution or reproduction is permitted
which does not comply with these terms.

Early diagenesis and benthic fluxes of redox-sensitive metals in eastern China shelf sediments

Xiaojing Wang^{1,2}, Li Li^{1,2,3*}, Yijun Ren¹, Peng Cao^{1,3}, Aimei Zhu^{1,2},
Jihua Liu^{1,2,3} and Xuefa Shi^{1,2,3}

¹Key Laboratory of Marine Geology and Metallogeny, First Institute of Oceanography, Ministry of Natural Resources, Qingdao, China, ²Key Laboratory of Deep Sea Mineral Resources Development, Qingdao, Shandong, China, ³Laboratory for Marine Geology, Laoshan Laboratory, Qingdao, China

Thirteen Short sediment cores (30–50 cm) were collected from Bohai Sea, Yellow Sea and Changjiang Estuary in China, and the early diagenesis of several redox sensitive metals (Fe, Mn, Mo, U and V, referring to as RSMs) in sediment were studied. The recycling process of Mo and Mn was closely correlated with each other, generating benthic fluxes diffusing upward from sediment to overlying water column, and the flux rates are related to the organic carbon oxidation rates. The recycling of U and V were more tightly coupled with Fe oxides, generating benthic fluxes going downward into the sediment in most cores. Significant authigenic accumulation of U, in contrary to little to no accumulation of Mo and V, were found in the study region, even in Changjiang Estuary where hypoxic condition was often found during summer. Benthic diffusive fluxes were compared with authigenic mass accumulate rates (MAR), which indicated that, besides the benthic diffusion process, there are other processes controlling the authigenic accumulation of the RSMs. The close relationships between authigenic accumulation of RSMs with OC_{burial} and OC_{burial} with S_{burial} , indicating the authigenic accumulation of RSMs is a consequence of redox environment in shelf sediment, which directly influencing the organic carbon degradation process. Compared with other continental margin, moderate enrichment of U was found in China continental sediment. The authigenic U accumulation in BS and NYS sediments accounted for 20 – 68% of the Yellow River input, whilst in SYS sediments accounted for ~ 64% of the Yellow River and Changjiang River input, which acting as important U sinks that cannot be ignored.

KEYWORDS

early diagenesis, redox sensitive metals, benthic flux, authigenic accumulation, eastern China marginal seas

1 Introduction

Redox sensitive metals (RSMs) such as iron (Fe), manganese (Mn), molybdenum (Mo), uranium (U), and vanadium (V) have been well-established as redox proxies in a wide range of coastal marine sediments (Mcmanus et al., 2005; Morford et al., 2005; McManus et al., 2006; Morford et al., 2009a; Abshire et al., 2020a; Abshire et al., 2020b). It is generally

accepted that RSMs are sensitive to redox conditions due to the different solubility of various species. The microbial-mediated remineralization of organic matter forms a major process that controls the redox conditions and the recycling of RSMs, often oxygen, NO_3^- , Fe/Mn oxides, SO_4^{2-} and CO_2 acting as electron acceptors, following certain thermodynamic order (Froelich et al., 1979; Emerson and Hedges, 2003). As a result of these early diagenetic reactions, RSMs that previously adsorbed with those biogenic/oxidized particles are released as dissolved phase, either diffused back to overlying water or accumulated into sediments by reduction (Shaw et al., 1990; Scholz et al., 2011; Li et al., 2021).

The eastern China seas are some of the most extensive shelf seas in the world, with shallow water depth and rapid sedimentation rates (Su and Yuan, 2005). Recently, studies have shown that hypoxia occurs in the bottom of the Bohai sea (BS) in summer, which is the result of stratification and the decomposition of organic matter (Zhao et al., 2017; Wei et al., 2019). The Changjiang Estuary (CJE) is one of the continental shelf areas with high primary productivity in the world. Regional and seasonal hypoxia often occurs off the Changjiang Estuary, usually begins in early June and may persist as late as October. Due to anthropogenic disturbance, excess riverine nutrient supply along with terrestrial materials has stimulated frequent coastal bottom-waters hypoxia events during summer (Chen et al., 2007; Chi et al., 2017). In recent decades, the minimum oxygen levels in the hypoxia zone did not show any decline, and the affected area has an enlarging trend (Wang, 2009; Zhu et al., 2011).

The eastern China continental shelf is reported to be an important sink for organic carbon (11–43%), while limited studies exist on early diagenesis and respiration processes of the RSMs (Zhao et al., 2021). Previous studies in northern Okinawa Trough, where oxic and suboxic sediment environment were found, has distinct enrichment of U but little accumulation for Mo, indicating that suboxic sediments act as an important sink for U, whilst anoxic environment is needed for the accumulation of Mo in sediments (Yamada et al., 2006; Wang et al., 2019). Xu (2007) and Wu et al. (2020) presented RSMs data of the Changjiang Estuary, and highlight the impact of seasonally hypoxic settings on the enrichment of Mo and V. However, for the vast majority areas of China continental shelves, the role of sediments as sinks or sources for RSMs has not been thoroughly investigated.

In this study, we collected 13 short (30–50 cm) sediment cores along the eastern China marginal seas, including Bohai and Yellow Seas and Changjiang estuary, which are characterized by rapid sedimentation rates and intense biological activities. Dissolved concentrations in porewater, overlying seawater and bulk contents in sediments (Fe, Mn, S, Mo, U, V) were measured to systematically understand the early diagenesis processes of RSMs. Benthic fluxes were estimated from one-dimensional diagenetic transport-reaction model, and compared with the authigenic RSMs accumulation rates, to qualitative and quantitative evaluate the processes that control the RSMs' recycling at sediment-water interface. The authigenic accumulation rates are compared with other marginal areas to establish a more synthetic view of RSMs behaviors along the eastern China margin.

2 Study area

The BS and Yellow Sea (YS) are two semi-enclosed continental seas of the northwestern Pacific Ocean located in the northeast of China, with a total area of $4.6 \times 10^5 \text{ km}^2$ and average depths of about 18 m and 44 m, respectively. The BS is enclosed by Liaodong and Shandong Peninsulas in northern China and connected to the YS through the narrow Bohai Strait. The YS is divided into the northern YS (NYS) and southern YS (SYS) by a boundary from Chengshanjiao of the Shandong Peninsula and Changshanchuan of the Korean Peninsula (Figure 1). Several rivers (Yellow River, Hai He and Luan He etc.) discharge along the coastal area of BS and YS, among which the Yellow River yields the largest sediment load ($\sim 1.1 \times 10^9 \text{ tons yr}^{-1}$) (Wang et al., 2007; Zhang et al., 2013). As shown in Figure 1, the hydrography of the study region is dominated by several southward local coastal currents, Yellow Sea Coastal Current (YSCC) and seasonally northward Yellow Sea Warm Current (YSWC) (Su and Yuan, 2005). YSWC is strongest in winter, and disappears or becomes weak in summer (Xu et al., 2009). With the onset of water stratification when the southwest monsoon prevails in late spring, Yellow Sea Cold Water (YSCW) forms, flourishing in summer and finally depressing in autumn (Hu, 1994; Zhang et al., 2008).

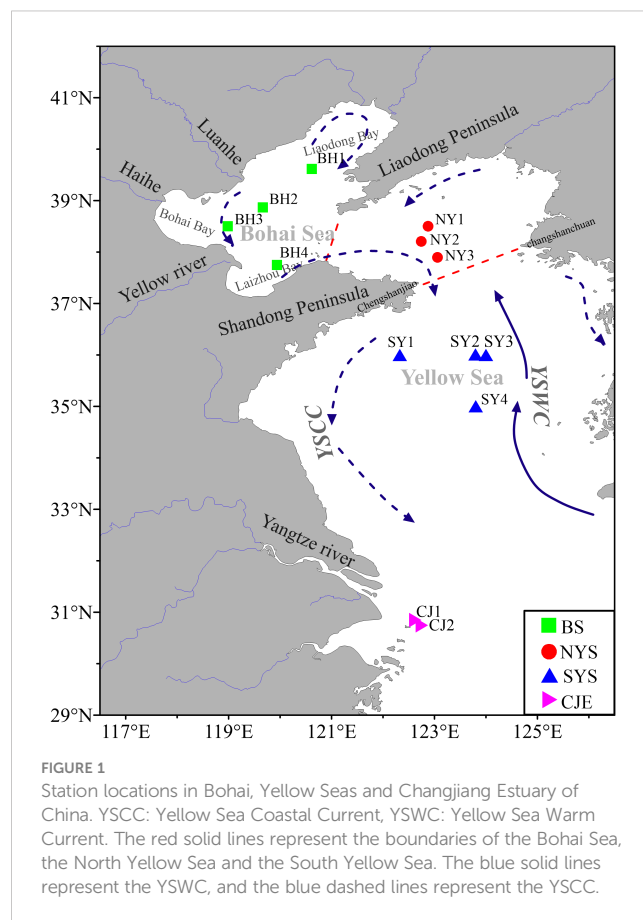


FIGURE 1
Station locations in Bohai, Yellow Seas and Changjiang Estuary of China. YSCC: Yellow Sea Coastal Current, YSWC: Yellow Sea Warm Current. The red solid lines represent the boundaries of the Bohai Sea, the North Yellow Sea and the South Yellow Sea. The blue solid lines represent the YSWC, and the blue dashed lines represent the YSCC.

3 Methods

3.1 Sample collection

Thirteen sediment cores (~ 20 - 45 cm) from the Bohai, Yellow Seas and Changjiang Estuary were collected onboard the *R/V Dongfanghong 2* (July, 2016), *R/V Zhedinyuyun* (August, 2017), *R/V Chuangxin 2* (July, 2018) and *R/V Xiangyanghong 18* (August, 2019), respectively. The sampling locations are shown in [Figure 1](#) and the information of the sites are reported in [Table 1](#). These cores were sampled using a box-corer at water depths of 15 to 77 m. Four cores (BH1-BH4) were located in the BS, three cores (NY1-NY3) in NYS, four cores (SY1- SY4) were in SYS and two cores (CJ1-CJ2) in CJE ([Figure 1](#)).

Upon collection, porewater was collected in a N₂-filled glove bag using Rhizon[®] sampler (Rhizonsphere Inc.) that was inserted into the pre-drilled holes on the cores, and Teflon lines and peristaltic pump (LongerParmer[®] Inc.) were coupled to form a trace-metal clean sampling system. The first mL of extracted porewater was discarded to prevent oxidation, collected samples were acidified to pH~2 with HNO₃ (Optima grade, Thermo Fisher Scientific Inc.) and stored at 4° C. Concurrently, parallel sediment cores were collected and sliced onboard the ship. Sediment samples were sealed in plastic bags and stored at 4°C until further processing. Sampling resolutions for porewater and sediment samples were 1 cm within the top 10 cm, and 2 cm for the remainder depth.

Bottom seawater samples (~ 2-5 m above the seafloor) were collected using Niskin bottles mounted on the CTD rosette. After

TABLE 1 Detailed information of the stations, and the measured TOC, CaCO₃, bottom water oxygen concentration ([O₂]_{bw}), along with the sedimentation rates, mass accumulation rates, organic carbon burial rate (OC_{burial}) used or calculated in this study.

Station	Sampling date	Water depth (m)	Bottom water temperature (°C)	[O ₂] _{bw} (μM)	TOC ^a (%)	CaCO ₃ ^b (%)	Sedimentation Rates (cm·y ⁻¹)	Mass accumulation rate (g·cm ⁻² ·y ⁻¹)	OC _{burial} (mmol·m ⁻² ·d ⁻¹)
BH1	July, 2016	29	12.2	289	0.47 ± 0.03	3.57 ± 0.57	0.29 ^c	0.33 ^c	3.51 ± 0.24
BH2	July, 2016	25	17.6	285	0.62 ± 0.04	3.69 ± 0.58	0.31 ^d	0.30 ^d	4.91 ± 0.30
BH3	July, 2016	23	16.8	262	0.43 ± 0.02	11.2 ± 1.45	0.20 ^e	0.20 ^j	1.98 ± 0.11
BH4	July, 2016	16	24.3	191	0.31 ± 0.05	11.8 ± 2.09	0.31 ^e	0.26 ^j	1.86 ± 0.28
NY1	July, 2016	58	7.3	339	0.54 ± 0.04	2.63 ± 0.42	0.09 ^f	0.07 ^f	0.86 ± 0.06
NY2	July, 2016	53	6.4	296	0.38 ± 0.04	3.82 ± 0.43	0.09 ^f	0.07 ^f	0.60 ± 0.07
NY3	July, 2016	61	6.7	301	0.29 ± 0.04	4.62 ± 0.54	0.08 ^f	0.07 ^f	0.45 ± 0.06
SY1	June, 2016	52	7.4	234	0.55 ± 0.03	5.35 ± 0.71	0.41 ^g	0.33 ^g	4.14 ± 0.21
SY2	August, 2019	72	7.9	182	1.02 ± 0.03	2.08 ± 0.44	0.17 ^g	0.14 ^k	3.16 ± 0.11
SY3	June, 2016	77	7.3	249	0.79 ± 0.04	3.82 ± 0.77	0.11 ^g	0.09 ^g	1.59 ± 0.09
SY4	August, 2019	76	8.3	198	0.58 ± 0.11	2.43 ± 0.69	0.06 ^g	0.05 ^k	0.64 ± 0.12
CJ1	July, 2018	21	27	111	0.46 ± 0.06	8.31 ± 0.45	0.34 ^h	0.36 ^l	3.82 ± 0.47
CJ2	August, 2017	27	21	174	0.38 ± 0.03	8.77 ± 0.43	2.40 ⁱ	2.57 ^l	22.4 ± 2.01

a: TOC contents are calculated average values from sediment samples deeper than 15 cm.

b: CaCO₃ contents are calculated average values of the whole sediment core.

c: Data from station B73 and BP1 in [Yang et al. \(1993\)](#).

d: Data from station M4-3 in [Li and Shi \(1995\)](#).

e: Data from station M8-4 and M8-12 in [Dong et al. \(1995\)](#).

f: Data from station C2 and NYS-5 in [Qi et al. \(2004\)](#).

g: Data from [Alexander et al. \(1991\)](#).

h: Data from station HN108 in [Xia et al. \(2004\)](#).

i: Data from station CJ08-689 in [Shi \(2014\)](#).

j: MAR are calculated based on the Eq. (5), the ρ_{dry} data are from station M8-4 and M6-3 in [Li and Shi \(1995\)](#), assumed to be 1.01 g·cm⁻³ and 0.85 g·cm⁻³ for BH3 and BH4.

k: MAR are calculated based on the Eq. (5), the ρ_{dry} data is from [Alexander et al. \(1991\)](#), assumed to be 0.80 g·cm⁻³.

l: MAR are calculated based on the Eq. (5), the ρ_{dry} data is from station SC07 in [Zhang et al. \(2009\)](#), assumed to be 1.07 g·cm⁻³.

collection, seawater samples were filtered immediately through 0.2 μm AcroPak[®] filters (Pall Inc.) into LDPE bottles (Nalgene[™], Thermo Fisher Scientific Inc.), and acidified to pH \sim 2 with HNO₃. Prior to the sampling, filters, bottles and other labware were thoroughly cleaned as described by Li et al. (2015).

3.2 Sample analysis

3.2.1 Seawater and porewater analysis

The seawater O₂ concentrations were determined onboard following the Winkler titration method (Grasshoff et al., 1999), the uncertainty was estimated to be $\pm 1 \mu\text{mol}\cdot\text{L}^{-1}$. Total dissolved sulfide (ΣHS^-) in porewater samples were determined on board inside a N₂-filled glove bag following the methylene-blue colorimetric method (Cline, 1969) with a UV spectrophotometer (7200 series, Shanghai Unico Inc., China). Sulfide standard solution and its dilution stabilizing solution (Beijing Aoke biotechnology Inc., China) were used to generate the calibration curves. The detection limit of the analytical method for sulfide was $1.9 \mu\text{mol}\cdot\text{L}^{-1}$.

Porewater and seawater samples were diluted 20-fold with 2% HNO₃ for analysis, only dissolved Mn in seawater samples were pre-concentrated using Nobias PA1[®] resin with a manually controlled manifold (Biller and Bruland, 2012). All samples were analyzed using ICP-MS under collision cell-mode (XII series, Thermo Fisher Scientific Inc.). Indium, Sc and Rh were added to all samples as internal standards. A random selection of 10% samples were spiked with metal standards to two increments concentrations to correct the sample matrix effects. The results showed that the recoveries for Fe, Mn, Mo, U and V were generally within 80 - 113%, and the porewater data of RSMs have been corrected by the recovery. Precision and accuracy of the method were tracked by analyzing certified reference materials (CASS-5 and NASS-6, National Research Council, Canada), and the results are shown in Table S1. The measured values were in good agreement with certified values.

3.2.2 Sediment analysis

Sediment samples (\sim 50 mg) were freeze-dried and digested with 3 mL mixed concentration acid (HNO₃: HF =1:1) at 190°C for 48 h, then diluted to 50 ml with 2% HNO₃. Al, Fe, Mn and S were analyzed by ICP-OES (iCAP 6300, Thermo Fisher Scientific Inc.) and Mo, U and V by ICP-MS. The recoveries of all metals were within 95-106% ($n = 20$) using sediment reference standards (GBW07309 and GBW07305a, China). Replicate analyses showed that the relative standard deviations (RSD) were $< 1\%$ for Al, Fe, Mn and S, and $< 5\%$ for Mo, U and V.

Total carbon (TC) and total organic carbon (TOC) were measured with an Elemental Analyzer (Model EL-III, Vario), and TOC samples were treated with 4 N HCl to remove inorganic carbon (TIC) before analysis. The recovery of TOC was 95-102% ($n = 10$) assessed by GBW07309, and the relative errors observed in triplicate analyses were $< 0.05\%$. Calcium carbonate content

(CaCO₃) was calculated from TIC according to molecular ratio of CaCO₃:C (100:12). Grain size were determined using a laser particle size analyzer (Master sizer 2000, Malvern Instrument), and categorized as clay ($< 4\mu\text{m}$), silt (4-63 μm) and sand ($> 63\mu\text{m}$).

3.3 Calculation of fluxes at the sediment-water interface (SWI)

Diffusive benthic fluxes of the RSMs at SWI and mass accumulation rates of authigenic metals (RSM_{AR}) in downcore sediments of coastal China were both calculated for the purpose of this study.

3.3.1 Diffusive benthic flux

The diffusive benthic fluxes across SWI were estimated using a one-dimensional transport-reaction model (Boudreau, 1997), which accounts for the effects of molecular diffusion, bioturbation and irrigation. The model takes the form:

$$\left(\frac{\partial C_{pw}}{\partial t}\right)_x = \frac{\partial}{\partial x} \left(\varphi(D_s + D_B) \frac{\partial C_{pw}}{\partial x} \right) + \varphi\alpha(C_o - C_{pw}) + R = 0 \quad (1)$$

where C_{pw} is the porewater concentration, C_o is the bottom water concentration, x is the depth, φ is the porosity, D_s is the molecular diffusion coefficient, D_B is the bioturbation coefficient, α is the irrigation coefficient, and R is the net rate of production per unit of sediment. No available irrigation coefficient (α) was found in the study area, therefore the irrigation process was not included.

The D_s was calculated by the Stokes-Einstein diffusion coefficient temperature dependence described by Li and Gregory (1974), adjusted to the bottom water temperature of 6.4 - 27°C. As there was no published D_{sw} (25°C) value for VO₄³⁻, we adopted the one of MoO₄²⁻ instead, because they exist in seawater as similar oxyanions (similar as in Scholz et al., 2011). Based on Eq. (2), the calculated D_s values ranged from $2.98 - 6.78 \times 10^{-6} \text{ cm}^2 \text{ s}^{-1}$ for Mn, $4.30 - 9.76 \times 10^{-6} \text{ cm}^2 \text{ s}^{-1}$ for Mo and V, $1.85 - 4.20 \times 10^{-6} \text{ cm}^2 \text{ s}^{-1}$ for U, respectively.

$$D_s = \frac{D_{sw}(25^\circ\text{C})}{2.19} + \frac{T}{25} \times (D_{sw}(25^\circ\text{C}) - \frac{D_{sw}(25^\circ\text{C})}{2.19}) \quad (2)$$

The D_B was calculated based on the formula from Tromp et al. (1995), as a function of the sedimentation rate (s), shown in Table 1:

$$\log_{10}(D_B) = 1.63 - 0.05 \cdot \log_{10}s \quad (3)$$

The benthic fluxes were calculated using the code PROFILE (Berg et al., 1998). The dissolved RSMs concentrations used for the bottom water (reported in Table 2) were positioned at 0.5 cm above seafloor in order to obtain the best fit between observed and modeled data. By definition, positive flux indicates diffusion upward into the overlying water, while negative flux is directed into the sediments. Strong advection flow could take place within sediments, ensuring a rapid exchange of solutes between burrows and overlying water. The calculated Peclet number are low (0.02-0.08), indicating

TABLE 2 Dissolved redox sensitive metal concentrations (unit: nmol L^{-1}) measured in bottom seawater in this study.

Station ID	Mn	Mo	U	V
BH1	22.0	112.7	12.6	42.1
BH2	27.1	110.8	12.7	43.2
BH3	21.1	110.8	12.7	43.2
BH4	23.3	113.1	13.8	43.8
NY3 ^a	20.5	108.4	12.3	42.6
SY1	5.90	106.4	12.9	41.7
SY3	4.45	113.0	12.6	46.7
CJ1	11.5	105.8	11.9	38.2
CJ2	16.9	94.9	12.5	44.7

a. The concentrations of dissolved RSM in NY3 are applied for the NY1 and NY2.

that the advection flux can be neglected relative to diffusion (Boudreau, 1997).

3.3.2 Mass accumulation rate (MAR) of authigenic metals

MAR of authigenic metals ($[Me]_{AR}$) were calculated based on Eq. (4):

$$[Me]_{AR} = MAR_{sed} \times [Me]_{auth} \quad (4)$$

where MAR_{sed} is the sediment mass accumulation rate, and $[Me]_{auth}$ refers to the average authigenic metals concentration, which was calculated as follows Eq. (5):

$$[Me]_{auth} = [Me]_{sample} - \frac{[Me]_{detr} [Al]_{sample}}{[Al]_{detr}} \quad (5)$$

where $[Me]_{sample}$ and $[Al]_{sample}$ are average bulk contents below 15 cm in each sediment core. The $[Me]_{detr} / [Al]_{detr}$ represents the ratio between detrital metal and detrital Al contents. The average metal contents of the local regional upper continental crust (UCC) values were used as the detrital values. Specifically, the UCC values of the northern margin of North China were used for BS and YS, and the UCC values of Changjiang for CJE (Gao et al., 1998). The S/Al detrital ratio in the northern margin of North China was not reported, the value in the Changjiang was adopted ($7.79 \times 10^{-3} \text{ g} \cdot \text{g}^{-1}$), which is closer to the UCC value reported by Rudick and Gao (2014).

For station BH1, BH2, NYS cores, SY1 and SY3, the MAR data are chosen from the reported MAR data from nearest locations. While for other cores, only sedimentation rates were found from the nearest locations in previous studies, therefore the MAR are calculated based on Eq. (6).

$$MAR_{sed} = s \times \rho_{dry} \quad (6)$$

where s is sedimentation rate and ρ_{dry} refers to the dry sediment density. All detailed information is reported in Table 1. Organic carbon burial rates (OC_{burial}) are calculated based on Eq. 7

$$OC_{burial} = C_{org} \times MAR \quad (7)$$

Where C_{org} is the average TOC content below 15cm in sediment core (Table 1), and the OC_{burial} results are shown in Table 1.

4 Results and discussion

4.1 Bottom water oxygen content

The bottom water oxygen concentrations ($[O_2]$) of the BS ranged from 191 μM to 289 μM (Table 1), comparable to the values previously reported in June to July in BS (average being $235 \pm 30 \mu\text{M}$; Wang et al., 2015). The bottom water $[O_2]$ in SYS (182-249 μM) were lower than that of the NYS (296-339 μM), and comparable to those reported in 35-36°N of China continental shelf during May to August (229-313 μM , averaged being 250 μM) (Sohrin et al., 1999; Chi et al., 2017). Although primary production consumed oxygen in surface water during spring to summer, seasonally northward flowing YSWC kept the bottom water oxygen concentrations still at a relatively high level in SYS (Hu, 1994; Wang, 1997).

4.2 Dissolved RSMs in porewater

4.2.1 Fe, Mn and S in porewater

The vertical distributions of Mn and Fe in porewater are shown in Figure 2. In SYS, dissolved Mn and Fe were negligible at the depth of 1-2 cm and increase to peak values by 3-10 cm, followed by a decrease downcore to constant values. Both Mn and Fe are known to be easily mobilized in reducing environment, and Fe peaks typically appear at a relatively deeper depth than Mn peaks (Figure 2), which is consistent with the expected thermodynamic order reported by Froelich et al. (1979). Similar dissolved Mn and Fe profiles were found in BH3 and NY3 cores (Figure 2). These cores indicate typical redox sequences of hemipelagic sediments, where a relatively oxidative sedimentary environment was found

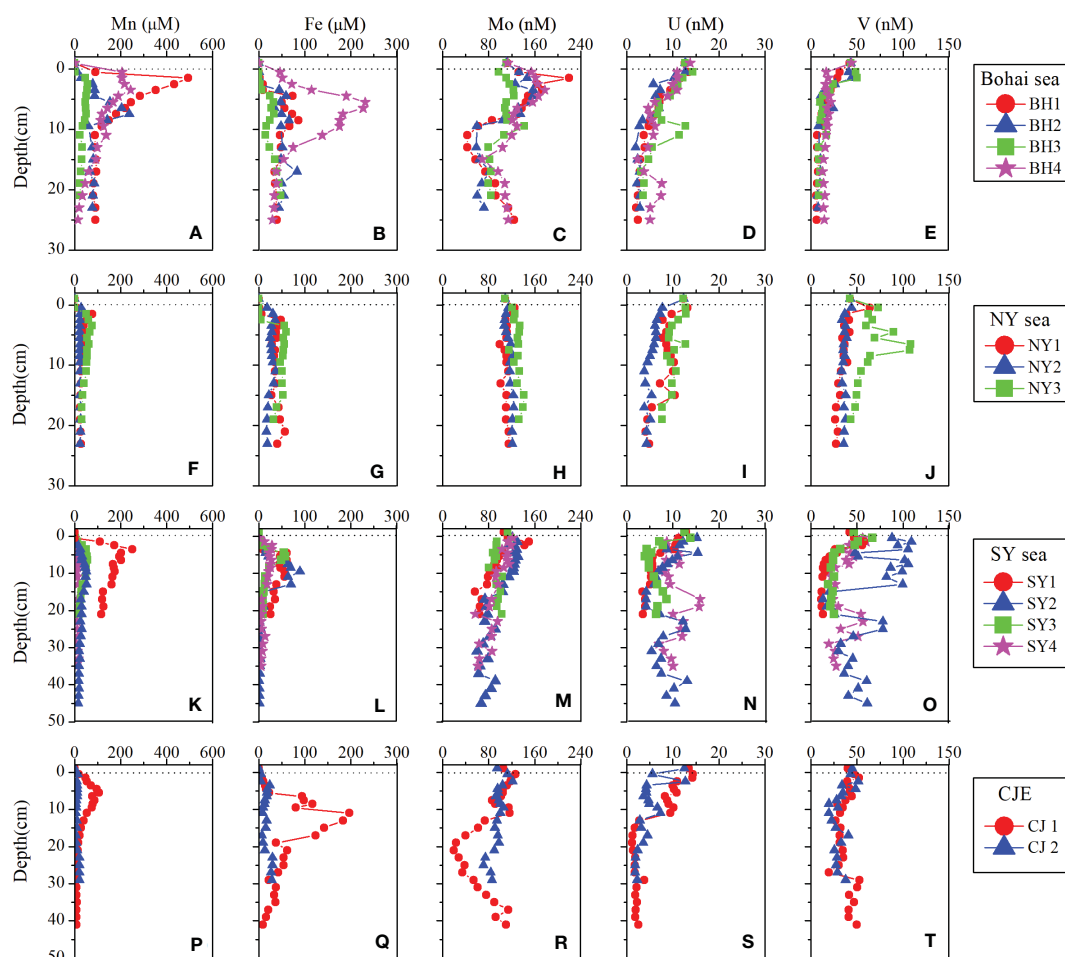


FIGURE 2

Porewater profiles for Fe, Mn, Mo, U and V for all cores. The dashed lines denote the sediment-water interface.

across the SWI (Shaw et al., 1990; Morford et al., 2005; Canfield and Thamdrup, 2009).

For other cores in the study area, dissolved Mn or Fe was measurable in surficial samples (Figure 2). Especially in cores near the coast, such as BH1, BH4 and NY2, dissolved Mn and Fe reached higher contents in the surface layer (28 - 205 μM for Mn, 18 - 46 μM for Fe). Higher dissolved Mn and Fe appear at or near-SWI, exhibiting a relatively reducing environment, especially in core BH4, consistent with the higher organic supply to the sediment and associated lower oxygen (191 μM) in the bottom waters.

According to the first appearance depth of dissolved Mn and Fe, sediments farther away from the coast were less reducible. Porewater profiles indicate that early diagenesis occurred mainly through the reduction of oxygen, Mn/Fe oxides, and no significant sulfate reduction was observed. Although no dissolved sulfide was measured (<1.9 μM) in any of the sediment cores, the formation of micro sulfide environment cannot be excluded. For example, at the bottom of SY2 and SY4 cores, dissolved Fe contents is significantly

reduced (1-2 μM and 5-7 μM , respectively) (Figures 2K, L), which may be affected by sulfide reduction.

4.2.2 Mo, U and V in porewater

Vertical distributions of dissolved Mo, U and V in porewater are shown in Figure 2. In most cores, dissolved Mo and V generally decrease with depth and approach constant concentrations at certain depths. Dissolved Mo and V showed one or two peaks in the Fe/Mn reduction zones (Figure 2), indicating that the recycling processes of Mo and V were coupled with Fe/Mn oxides (Morford and Emerson, 1999; Morford et al., 2005; Whitmore et al., 2019). Below the Fe/Mn oxides reduction zone, V(V) is progressively reduced to V(IV) and, if H_2S is present, to V(III) (Wehrli and Stumm, 1989; Wanty and Goldhaber, 1992). Reduced V is removed from porewater by surface adsorption of organic V(IV) complexes, formation of insoluble V(III) oxides and incorporation of V(III) into insoluble organic compounds (Wanty and Goldhaber, 1992). Reduction of Mo (VI) to Mo (IV) occurs under sulfidic conditions ($\text{H}_2\text{S} > 0.1 \mu\text{M}$), molybdate is subsequently transformed into

thiomolybdates ($\text{Mo}_4\text{S}_{4-x}^{2-}$, $x=0$ to 3) (Helz et al., 1996; Zheng et al., 2000) and finally scavenged as particle-reactive thiomolybdate (MoS_4^{2-}) by Fe sulfides and/or sulfur-rich organic materials (Tribouillard et al., 2004; Vorlicek et al., 2004).

Dissolved U showed significant removal from porewater, from 10–13 nM at the top to 2–6 nM below 15 cm in most cores. The prominent curvature of porewater U was coincident with the depth of the dissolved Fe peaks (Figure 2). Dissolved U exists as carbonate complex that does not adsorb to Mn/Fe oxides or any other inorganic particles in the water column. Reduction of U(VI) to U(IV), a process that usually occurs at or below the depth of Fe remobilization. Mediated by Fe and sulfate-reducing bacteria, reduced U is removed from porewater by adsorption or precipitation of U oxides (Lovley et al., 1991; Zheng et al., 2002).

For some cores, besides the subsurface peaks in Mn/Fe reduction zone, deeper peaks of dissolved Mo, U and V in BH3, NY3, SY2 and SY4 were also found (Figure 2), which may be related to the regeneration of authigenic metals caused by bioturbation or bioirrigation oxidative dissolution (Aller, 1980; Morford et al., 2009a). This is supported by the findings of shell fragments at 10–14 cm depths in NY3 and SY4 cores and biological burrows at the surface layer of core BH3. In BH1, BH4 and CJ1 cores, with broader Fe peaks below the Mn peaks, dissolved Mo decreased to ~40 nM from 2 to ~15 cm, then increased to ~120 nM by the cores bottom (Figures 2C, R). The removal of Mo from porewater in the Mn reduction zone most likely occurs when Fe(II) is oxidized by Mn(IV) (Burdige, 1993; Postma and Appelo, 2000), causing dissolved Mo released from the Mn oxides may immediately be re-adsorbed to the fresh Fe hydroxides surfaces (Gustafsson, 2003; Goldberg et al., 2009). Upon burial deeper into the Fe reduction zone, Mo is released back into the porewater as Mo-rich Fe hydroxides dissolves (Herbert et al., 2020), resulting in the porewater Mo increases gradually.

4.3 Elemental distribution in sediments

4.3.1 TOC, grain size

The sediment types varied from silty sand to clayey silt (Figure S1). Most core sediments fell into the clayey silt domain, while BH1, NY1 and NY3 were sandy silt and silty sand. The average TOC contents ranged from 0.22% to 1.08%, higher TOC contents (0.65–1.08%) were found in SYS (Table 1). Vertically, the TOC content decreased within the top few cm, then remained constant (Figure S2). For most cores, averaged TOC contents were correlated well with mean grain size (Mz) ($P < 0.01$), but not for BH3, BH4 and CJ2 (Figure S3). These cores have higher CaCO_3 contents (8–11%) (Table 1), and the insignificant linear correlation may be caused by the source-dependent control (e.g., Yellow River and Changjiang River input) (Bigot et al., 1989; Qiao et al., 2010).

4.3.2 Solid phase RSMs

Vertical distributions of Mn, Fe, S, Mo U and V are shown in Figure 3. All data were normalized by Al to minimize the grain size effect (Roussiez et al., 2005; Hu et al., 2013). To elucidate the relationships among the RSMs, TOC, S and Mz in sediments,

Spearman correlation analysis was performed, and the results are shown in Table S3. Again, all data are normalized to Al to minimize the grain size effect for the correlation analysis.

First of all, Fe exhibited a nearly invariant distribution with depth for all cores. Fe/Al in sediments were correlated well with Mz and TOC ($n = 256$, $p < 0.01$), indicating the recycling processes of Fe was associated with Mz and TOC. Unlike Fe, Mn has obvious enrichment in surface sediment in all study regions except CJE sites. The enrichment is most obvious at the sites near the Shandong Peninsula (Figure 3M), which was similar to previous reported data here (Yuan et al., 2012). Except for BH1 and BH2 cores, averaged Mn/Al for whole cores were correlated well with CaCO_3 ($r^2 = 0.68$, $p < 0.01$). The mechanism is probably due to the sediments dominated by high content of CaCO_3 originated from riverine input and biogenic CaCO_3 , such as shell fragments (Yang et al., 2003), while dissolved Mn can be adsorbed on, or incorporated into, freshly precipitated CaCO_3 in seawater and settled in sediment (Aller and Rude, 1988; Kim et al., 1998). Other studies have also found that high contents of Mn in surficial sediments were related to up-diffusion Mn(II) reoxidation by the reduction of Mn oxides in deeper sediments (Nolting et al., 1996; Mouret et al., 2009; Volz et al., 2020), which is in agreement with the observation that the cores with higher surface Mn corresponding to higher dissolved Mn peaks in porewater (Figures 2, 3), indicating the influence of diagenetic process.

In surface sediments, Mo peaks often resonate with Mn peaks (Figure 3), confirming that Mo recycling process is associated with Mn in oxic layer (Morford and Emerson, 1999; Sundby et al., 2004; Li et al., 2020). The average Mo/Mn ratio is $\sim 0.001 \pm 0.0002$ ($n = 29$) in Mn-enriched layer (≤ 5 cm), comparable to the ratio for oxic sediments in North American Arctic margin (~ 0.001) (Kuzyk et al., 2017), slightly lower than the ratio observed worldwide (~ 0.002) (Shimmield and Price, 1986; Chaillou et al., 2002). While below the Mn-enriched layer (> 5 cm), significant correlations were found between Mo/Al - S within most cores ($r^2 = 0.40 - 0.92$, $p < 0.01 - 0.05$). It is generally accepted that Mo precipitation in reducing sediments is related to the balance between Fe and sulfate reduction (Zheng et al., 2000; Morford et al., 2009a). Kang et al. (2014) observed that S_{total} and S_{reduced} gradually increased with depth in YS and CJE sediments, and pyrite -S was the predominant reduced inorganic sulfur phase. Probably, dissolved Mo removed from porewater was directly trapped by reduced S and subsequently accumulates as a Mo-Fe-S phase (Zheng et al., 2000; Helz and Vorlicek, 2019).

Solid U remains roughly detrital level (~ 1.23 $\mu\text{g/g}$ for BH and YS, ~ 1.40 $\mu\text{g/g}$ for CJE) within top 5–10 cm in most cores, with enrichment occurring at deeper depth (Figure 3). Previous studies have reported that U accumulation is sensitive to OC delivery to the seabed (Anderson et al., 1989; Zheng et al., 2002). A weak correlation between U/Al - TOC was found, while U/Al and S/Al showed a good correlation ($r^2 = 0.43$, $n = 256$, $p < 0.01$) (Table S3). Normally U does not form stable sulfides, but free sulfide may promote reduction/fixation of U (Emerson and Husted, 1991). However, no vertical variation of solid U was found in CJE cores (Figure 3W), which is consistent with the results reported by Scholz et al. (2011) and Wu et al. (2020), possibly related to seasonal oxygen fluctuations in bottom water. In such settings, authigenic U precipitated during reducing periods undergoes transient re-oxidation, and correspondingly leads to the erasure of the accumulated signal.

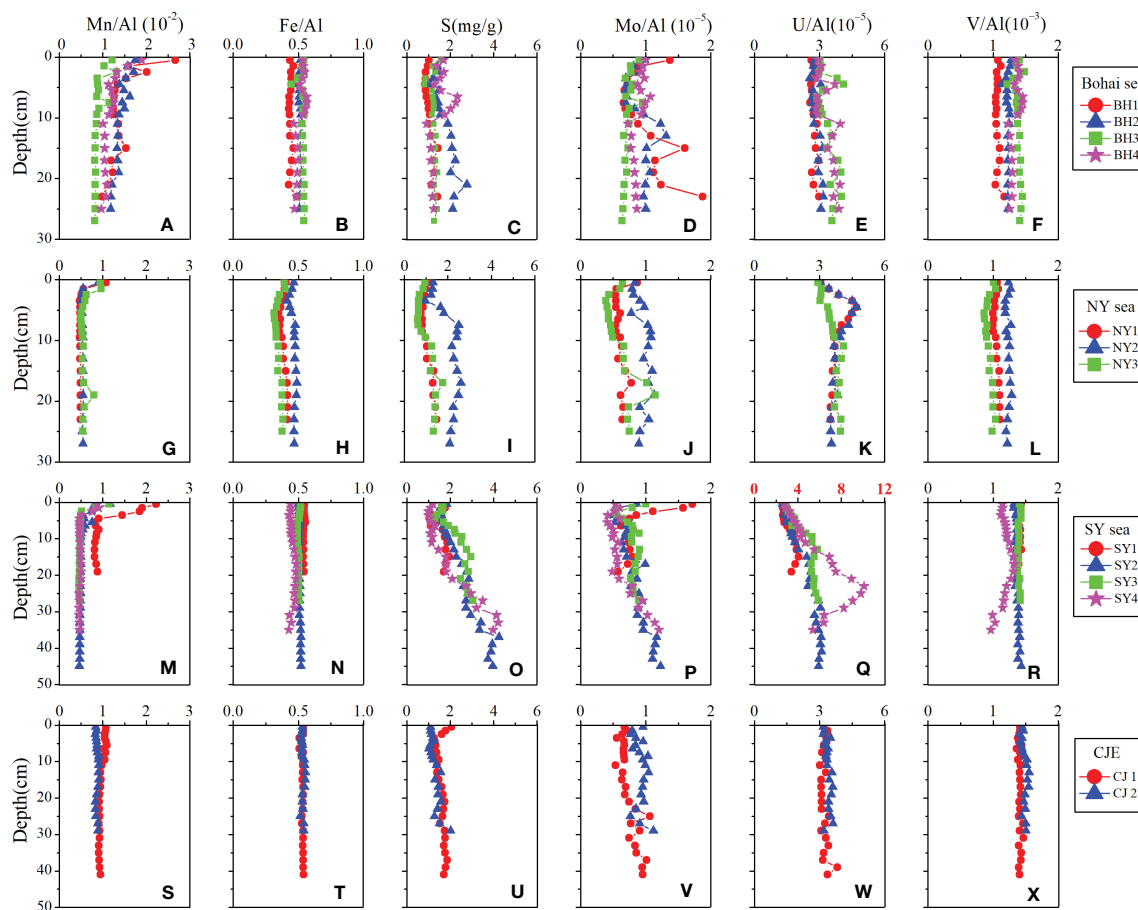


FIGURE 3
Solid phase profiles of trace metal in sediment cores.

In most cores, solid V parallel the vertical distribution of Fe (Figure 3). Various studies have well-described the scavenging of V (V) is associated with particulate Fe and Mn by either adsorbed or incorporated, and particulate Fe may have more control over V cycling than Mn in shelf sediments (Scholz et al., 2011; Whitmore et al., 2019; Li et al., 2020). Significant correlations between V/Al - Fe/Al ($r^2 = 0.87$, $p < 0.01$, Table S3) was observed, which confirmed the co-cycling of V with Fe. The close correlations were also found between V/Al, mean grain size (Mz) and TOC ($n = 256$, $p < 0.01$, Table S3), which has been observed in various marine environments (Wang et al., 2019; Li et al., 2020; Wu et al., 2020). This suggests that the accumulation of V in sediments is also related to TOC and grain size, and Li et al. (2020) found that TOC may only play a role at low levels ($< 1\%$), which is consistent with our low TOC content sediments (0.10 - 1.29%).

4.4 Benthic fluxes and authigenic accumulation of RSMs

Based on the method described in section 3.3, the benthic fluxes of RSMs were calculated and compared with calculated

[RSM]_{AR} in sediments, and the results are shown in Figure 4 and Table S4.

4.4.1 U

As shown in Figure 4, U had benthic fluxes going into the sediments, the estimated fluxes were 0.83 - 6.36 $\text{nmol}\cdot\text{m}^{-2}\cdot\text{d}^{-1}$, with an average of $3.02 \pm 1.74 \text{ nmol}\cdot\text{m}^{-2}\cdot\text{d}^{-1}$. The diffusive fluxes were comparable to that reported from the Changjiang estuary (1.10 - 2.19 $\text{nmol}\cdot\text{m}^{-2}\cdot\text{d}^{-1}$), continental shelf of central California (2.30 - 9.90 $\text{nmol}\cdot\text{m}^{-2}\cdot\text{d}^{-1}$) and central China ($5.21 \pm 2.74 \text{ nmol}\cdot\text{m}^{-2}\cdot\text{d}^{-1}$) (Zheng et al., 2002; Zou et al., 2010; Wang et al., 2019). U_{AR} in sediments were 8.68 - 331.7 $\text{nmol}\cdot\text{m}^{-2}\cdot\text{d}^{-1}$, with an average of 53.0 $\text{nmol}\cdot\text{m}^{-2}\cdot\text{d}^{-1}$. NYS is the only region where benthic fluxes were in agreement with U_{AR} . In other regions, U_{AR} were 1-2 orders of magnitude higher than diffusive fluxes (Table S4).

The fraction of U_{AR} in sediment reflects not only the input from diffusion across the SWI (U_{diff}) and particulate non-lithogenic uranium (U_{PN}), but also the loss caused by U remobilization (U_{remob}) (Zheng et al., 2002). A mass budget for U is calculated as:

$$U_{AR} = U_{diff} + U_{PN} - U_{remob}$$

U_{PN} is preserved at $O_2 < 25 \mu\text{M}$ (Zheng et al., 2002), therefore U_{PN} was thought to be negligible for U_{AR} . The discrepancy between

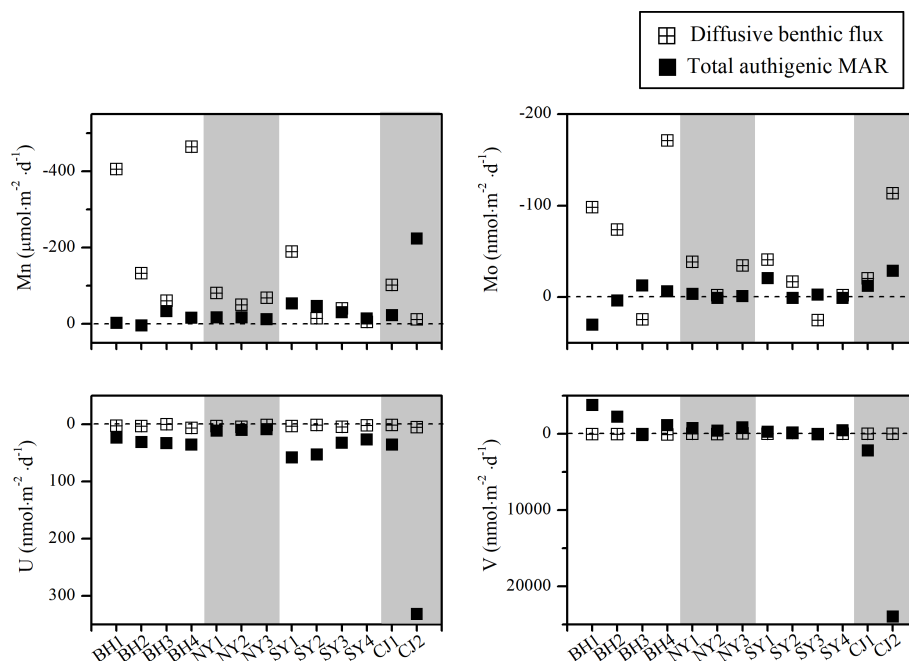


FIGURE 4

Diffusive benthic fluxes and authigenic MARs in sediment cores against stations. Horizontal dashed lines represent SWI. Grayish and whitish arrays represent BS to CJE.

U_{diff} and U_{AR} may be related to the bioturbation or bioirrigation, which can significantly influence the transport of solutes in sediments and enhance benthic flux (Morford et al., 2007; Morford et al., 2009b). Previously accumulated U can be released to bottom water or porewater by oxidation of reduced U in sediments (Zheng et al., 2002; Morford et al., 2009b), resulting in the loss of authigenic U, such as BH1 and BH2 cores with lower authigenic U ($0.62 \mu\text{g}\cdot\text{g}^{-1}$ and $0.89 \mu\text{g}\cdot\text{g}^{-1}$, respectively). For some cores, partial remobilized U may diffuse downward into deeper and more reducing sediment, causing secondary precipitation and increasing accumulation in sediments (Morford et al., 2007; Costa et al., 2018).

Studies have found that U_{AR} is sensitive to the organic carbon flux (rain, oxidation or burial) (Zheng et al., 2002; Mcmanus et al., 2005; Kuzyk et al., 2017). Significant positive correlations were observed between the average U_{AR} with OC_{burial} and S_{AR} ($p < 0.01$) (Figures 5A, B), indicating that the coastal sediment is not only an effective sink for organic carbon but also for U. Meanwhile, OC_{burial} was correlated well with S_{AR} (Figure 5C), indicating that the coupling of TS and TOC controls the accumulation of U in downcore sediments. Overall, these relationships highlight the potential utility for authigenic U as a rough proxy to reconstruct the sedimentary redox condition in marine systems.

4.4.2 Mo

At most sites, benthic Mo fluxes (-2.26 - $-171.3 \text{ nmol}\cdot\text{m}^{-2}\cdot\text{d}^{-1}$) leave the sediments and enter the overlying water (Figure 4), with an average of $-55.8 \pm 53.2 \text{ nmol}\cdot\text{m}^{-2}\cdot\text{d}^{-1}$. The estimated average Mo

benthic flux was 1-2 orders of magnitude lower than those reported in other coastal sediments overlying oxic bottom water, such as Buzzards Bay ($-301 \pm 225 \text{ nmol}\cdot\text{m}^{-2}\cdot\text{d}^{-1}$) and central Baltic Sea (-200 - $-2000 \text{ nmol}\cdot\text{m}^{-2}\cdot\text{d}^{-1}$), with water depths less than 60 m (Morford et al., 2009a; van de Velde et al., 2020).

Previous studies have indicated the close relationship between Mo and Mn, not only in surface sediment enrichment, but also in benthic fluxes (Morford and Emerson, 1999; Sundby et al., 2004; Scholz et al., 2011). A significant correlation was found between the benthic fluxes of Mo and Mn ($r = 0.86$, $p < 0.01$, $n = 10$), which provides supplementary evidence to support coupled recycling relationship between Mo and Mn in oxic sediments. In addition, since Mn is scavenged by organic matter in seawater and settled on surface sediments (Johnson et al., 1996), organic carbon respiration exerts some primary control over the Mn flux at SWI (McManus et al., 2012; Hyun et al., 2017). Speculation thus exists that Mo fluxes may have similar behavior. Significant linear relationships between benthic fluxes of Mn and Mo and the respiration rates were found ($p < 0.01$, $n = 10$) (Figures 6A, B), indicating benthic Mn and Mo fluxes are associated with the organic carbon oxidation rate in coastal areas.

Few or no authigenic Mo_{AR} was found in this study (Figure 4). Authigenic Mo accumulation seems to depend on the presence of organic matter flux and sulfate reduction (Chaillou et al., 2002; Dale et al., 2012). As described by Morford et al. (2005) and Helz and Vorlicek (2019), the increase in organic carbon flux promotes the accumulation of Mo due to the coupling between organic carbon and sulfur burial. Authigenic Mo accumulation was found in core

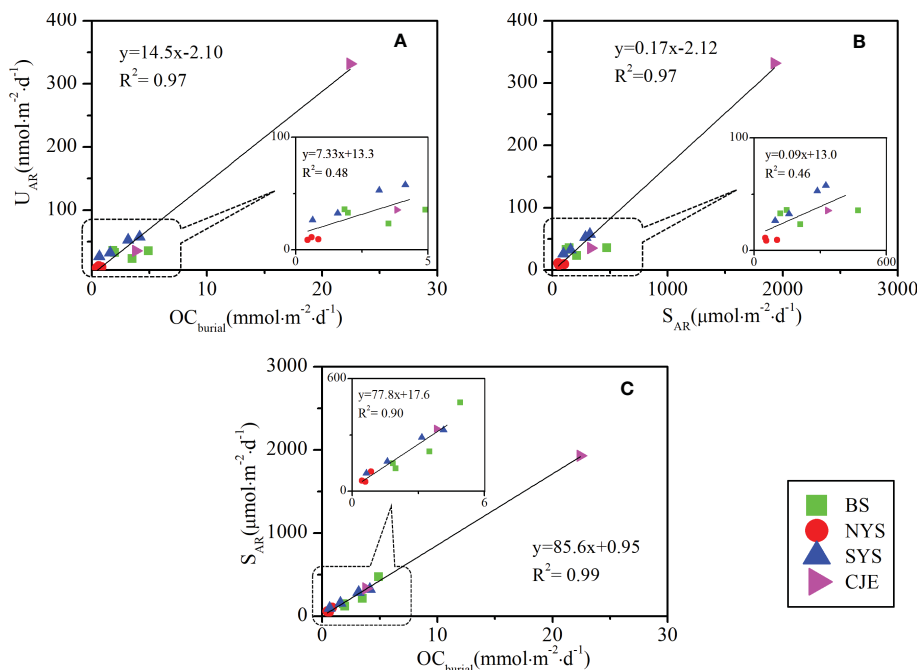


FIGURE 5 Relationship between U accumulation rates (A) with organic carbon burial rates; (B) with sulfur accumulation rates. (C) Sulfur accumulation rates with organic carbon burial rates. The imbedded figures are enlarged dataset without the data of station CJ2.

BH1, BH2, SY2 and SY4, accompanied by relatively high TOC burial and authigenic S (Table S4). Previous studies have reported that the amounts and reactivity of TOC were the major limiting factors for sulfate reduction in YS and CJE sites (Panutrakul et al., 2001; Kang et al., 2014), which may further limit the accumulation of authigenic Mo.

4.4.3 V

As shown in Figure 4, V diffused downward into the sediments in most cores, ranged from 2.28 to 74.2 nmol·m⁻²·d⁻¹, with an

average of 23.7 nmol·m⁻²·d⁻¹. The downward fluxes of V were relatively low compared to those reported along the Peruvian continental sediments covered by suboxic - anoxic bottom water (169 - 256 nmol·m⁻²·d⁻¹) (Scholz et al., 2011).

In most cores, solid V exhibited significant depletion (~ 10 - 30%) of the detrital content, which were comparable to that found in coastal-reducing sediment (Morford and Emerson, 1999). While for the cores near the estuary (BH3, CJ1 and CJ2), authigenic V accumulation were found in sediments (162 - 23977 nmol·m⁻²·d⁻¹), and the calculated V_{AR} were significantly higher than the benthic

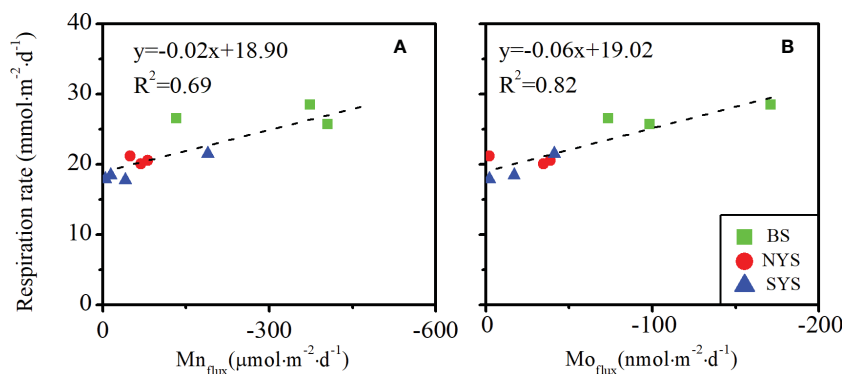


FIGURE 6 Relationship between benthic respiration rate and (A) benthic Mn flux; (B) benthic Mo flux. Core BH3, CJ1 and CJ2 are excluded from the diagrams, which are subject to strong hydrodynamic.

fluxes (Table S4), which should be caused by other processes supplying V to the sediments. As discussed in section 4.3, V adsorption onto Fe oxides may be the dominant mechanism for authigenic V accumulation in sediments, (Morford and Emerson, 1999; Whitmore et al., 2019; Li et al., 2020). Meanwhile, in reductive environment, authigenic V accumulation is primarily sensitive to the delivery and burial of organic matters (Wang and Wilhelmy, 2009; Li et al., 2020). However, most cores have no V authigenic accumulation (Figure 4), possibly due to the low TOC burial.

Significant V_{AR} depletion and higher upward diffusive flux ($-47.9 \text{ nmol}\cdot\text{m}^{-2}\cdot\text{d}^{-1}$ - $-92.9 \text{ nmol}\cdot\text{m}^{-2}\cdot\text{d}^{-1}$) were found in NY3 and SY2 cores (Table S4), corresponding to high V concentrations above 10 cm in porewater (51.3 - 109 nM) (Figures 2J, O). Under moderate reducing conditions, V(V) is reduced and present as particle-reactive V(IV), preferentially retained in porewater and diffused upward, likely due to forming dissolved metal-organic complexes (Wehrli and Stumm, 1989; Olson et al., 2017), indicating the influence of DOC on mobilization of V from sediments.

TABLE 3 Bottom water oxygen concentration ($[O_2]_{bw}$), oxygen penetration depth ($[O_2]_{pen}$), organic carbon burial rate (OC_{burial}) and authigenic accumulation rates of RSMs in this study, compared with those data reported from other coastal sediments worldwide.

Region	$[O_2]_{bw}$ μM	$[O_2]_{pen}$ (cm)	OC_{burial} $\text{mmol}\cdot\text{m}^{-2}\cdot\text{d}^{-1}$	S_{AR} $\text{mmol}\cdot\text{m}^{-2}\cdot\text{d}^{-1}$	Mo_{AR} $\text{nmol}\cdot\text{m}^{-2}\cdot\text{d}^{-1}$	U_{AR} $\text{nmol}\cdot\text{m}^{-2}\cdot\text{d}^{-1}$	V_{AR} $\text{nmol}\cdot\text{m}^{-2}\cdot\text{d}^{-1}$	Reference
Bobai Sea	191 - 289		2.92 ± 1.20	0.22 ± 0.13		30.7 ± 5.29		this study Song et al., 2020
North Yellow Sea	296 - 339		0.64 ± 0.21	0.07 ± 0.03		9.76 ± 1.23		
South Yellow Sea	182 - 249		2.38 ± 1.57	0.22 ± 0.11		42.3 ± 15.2		
Changjiang Estuarine	111 - 174	0.2 - 0.3	13.1 ± 13.2	1.13 ± 1.13		183 ± 209	13084 ± 15404	
Calculated averages			3.80 ± 5.77	0.33 ± 0.50		52.9 ± 85.1	1245 ± 6964	
Northern Okinawa Trough					1.10 ± 5.48	11.2 ± 6.84		Wang et al., 2019
NE Pacific margin off Washington/Oregon	40 - 55	0.3 - 0.5	0.3			0.58 - 0.62		Stump and Emerson, 2001; Morford et al., 2005
	81 - 124	1.5 - 5	0.01 - 0.04			0		
Pacific margin off California	3 - 27	0.2 - 0.6	1.2 - 2.6		6.0 - 22	9 - 11		McManus et al., 2005; McManus et al., 2006
	65 - 132	1.3 - 2.9	0.08 - 0.9		0 - 0.6	0.4 - 6		
Mexican margin	0 - 0.2		1.7 - 8.4		30 - 134	11 - 51		
Peru margin	< LD				85 - 443	18 - 21	712 - 986	Scholz et al., 2011
	4.2 - 42				9.6 - 74	30 - 57	82 - 356	
Laurentian Trough, eastern Canadian continental margin	75 - 365	0.4 - 1.0	1.0 - 20		7.1 - 219	4.7 - 36		Sundby et al., 2004 Morford et al., 2007; Morford et al., 2009b
	247 - 271	1.4 - 4.0	0.7 - 5.5			4 - 13		
Southern margin of the Arctic					40.0 ± 24.8	6.91 ± 4.43		Kuzyk et al., 2011
North American Arctic margin				0.87 ± 0.28	202 ± 47.2	58.3 ± 23.6		Kuzyk et al., 2017
				0.07 ± 0.12	23.8 ± 36.3	18.6 ± 14.8		
East Siberian Arctic Shelves			3.50 ± 0.31	0.29 ± 0.12	58.5 ± 2.02	24.2 ± 3.26	3223 ± 76.0	Li et al., 2020

4.5 The budgetary implications of authigenic RSMs

Changes in oxygen penetration depths, OC_{burial} and S_{AR} determine the accumulation rate of authigenic RSMs, however, the extent for Chinese coastal sediments acts as a sink or source of authigenic RSMs is unclear. What is needed is a comparison with those reported in other margin sediments. As shown in Table 3, except for CJE, moderate authigenic U accumulation rates were found in sites from BS to SYS. Previous studies have found that oxygen penetration depth is relatively less important for RSMs accumulation compared to OC_{burial} , and U_{AR} can vary by over a factor of 40 in sediments with oxygen penetration depth ≤ 1 cm (Mcmanus et al., 2005; Morford et al., 2009b). However, authigenic Mo has little or no accumulation in study area, much lower than that in anoxic sediments such as Peru and North American Arctic margin. By contrast, significant authigenic accumulation of Mo and V require sufficient reducing environment and high burial of TOC and sulfur. The spatial variability of authigenic RSMs accumulation rates was revealed, providing a reference for accurately estimating the importance of the continental sediments of China in global budgets.

The amount of U_{AR} were estimated, averaged to be 2.05 ± 0.35 , 0.60 ± 0.08 and $11.0 \pm 3.97 \times 10^8 \text{ g}\cdot\text{y}^{-1}$ in BS, NYS and SYS (given the areas being $7.7 \times 10^4 \text{ km}^2$, $7.1 \times 10^4 \text{ km}^2$ and $3.0 \times 10^5 \text{ km}^2$, respectively) (Qin et al., 2011; Shi, 2014). Among the rivers flowing to the coastal of eastern China, the Yellow River is the primary sources of sediment for the BS and NYS, while the SYS is mainly derived from the Yellow River and Changjiang River. Riverine input of dissolved U from the Yellow River and Changjiang River were 3.03×10^8 and $1.41 \times 10^9 \text{ g}\cdot\text{y}^{-1}$, respectively (Qu et al., 1993; Dunk et al., 2002). Compared with the riverine input, the U_{AR} in BS and NYS shelf sediments accounts for $\sim 67\%$ and $\sim 20\%$ of the Yellow River input, while the accumulation of U_{AR} in SYS shelf sediment accounts for $\sim 64\%$ of the Yellow River and Changjiang River input combined.

In general, the results show that the costal sediments of China are important sinks for U, which play a key role in balancing the global U budget (Barnes and Cochran, 1990; Wang et al., 2019), which has never been studied before. Notably, after the impoundment of the Three Gorges reservoir and Xiaolangdi reservoir in Changjiang and Yellow River, sediment loads from rivers decreased dramatically (Wang et al., 2007), resulting in the OC burial greatly reduced (64 - 68%) in East China coastal sediments (Zhao et al., 2021). This will alter the ability of the China continental sediments to act as important sinks for OC, as well as RSMs.

5 Conclusion

This study has collected short sediment cores in Bohai Sea, Yellow Sea and Changjiang Estuary. The RSMs in porewater and solid-phase were studied, and the benthic diffusive flux and authigenic mass accumulation rate were calculated based on the observed data. First of all, the environment at sediment-water

interface was found to be oxic or suboxic. Statistical analysis showed that the recycling process of Mo, U, and V was impacted by the recycling process of Fe/Mn oxides. The benthic fluxes of Mn and Mo were found to be going out of the sediments into overlying water column, while the fluxes of U and V were the opposite, going into sediments from overlying water column.

Comparison of benthic diffusive flux with MAR showed that Mo and V fluxes are independent of the authigenic accumulation rates, and U fluxes matched only in direction, indicating that there are other processes, besides the benthic diffusion, control the authigenic RSMs accumulation. Close relationship was found between the authigenic accumulation of RSMs and OC_{burial} , implying that the authigenic accumulations of RSMs is closely related with the organic carbon degradation process. Compared with other worldwide continental margins, moderate enrichment of U was found in northern China continental sediments. The estimated authigenic U fluxes in the study region accounted for approximately 20 - 68% of the Yellow River input in BS and NYS and $\sim 64\%$ of the Yellow River and Changjiang River in SYS, playing an important role in balancing the global U budget. Due to limited sampling stations, these 13 sediment cores may not be fully representative of each region's characteristic. However, they did show regional differences, and it cannot be ignored that the coastal sediments in China acts as an important sink for U globally.

Data availability statement

The original contributions presented in the study are publicly available. This data can be found here: <https://dx.doi.org/10.13140/RG.2.2.26194.63681>.

Author contributions

XW and LL designed the research. XW, YR, PC and AZ contributed sample collection, sample analysis, and data discussion. XW, LL and JL analyzed the data. XW, LL and XS wrote the manuscript. All authors contributed to the article and approved the submitted version.

Funding

This work is funded by the Marine S&T Fund of Laoshan Laboratory (LSKJ202204200) and the National Natural Science Foundation of China (42076046, 41776095, 41806082).

Acknowledgments

We would like to thank the captain and crew of the *R/V Dongfanghong 2*, *R/V Zhedinyuyun*, *R/V Chuangxin 2* and *R/V Xiangyanghong 18* for their support at sea. We also want to thank all the graduate students who have helped at sea or in the laboratory to make this work possible, especially Hongna Liu and Xiaotong Zhen.

Conflict of interest

The authors declare that the research was conducted in the absence of any commercial or financial relationships that could be construed as a potential conflict of interest.

Publisher's note

All claims expressed in this article are solely those of the authors and do not necessarily represent those of their affiliated

organizations, or those of the publisher, the editors and the reviewers. Any product that may be evaluated in this article, or claim that may be made by its manufacturer, is not guaranteed or endorsed by the publisher.

Supplementary material

The Supplementary Material for this article can be found online at: <https://www.frontiersin.org/articles/10.3389/fmars.2023.1154248/full#supplementary-material>

References

- Abshire, M. L., Owens, J. D., Cofrancesco, J., Inthorn, M., and Riedinger, N. (2020a). Geochemical signatures of redepositional environments: the Namibian continental margin. *Mar. Geol.* 429, 106316. doi: 10.1016/j.margeo.2020.106316
- Abshire, M. L., Romaniello, S. J., Kuzminov, A. M., Cofrancesco, J., Severmann, S., and Riedinger, N. (2020b). Uranium isotopes as a proxy for primary depositional redox conditions in organic-rich marine systems. *Earth Planet. Sci. Lett.* 529, 115878. doi: 10.1016/j.epsl.2019.115878
- Alexander, C. R., Demaster, D. J., and Nittrouer, C. A. (1991). Sediment accumulation in a modern epicontinental-shelf setting: the yellow. *Sea. Mar. Geol.* 98 (1), 51–72. doi: 10.1016/0025-3227(91)90035-3
- Aller, R. C. (1980). Diagenetic processes near the sediment-water interface of long island Sound. II. Fe and Mn. *Adv. Geophys.* 22, 237–350. doi: 10.1016/S0065-2687(08)60067-9
- Aller, R. C., and Rude, P. D. (1988). Complete oxidation of solid phase sulfides by manganese and bacteria in anoxic marine sediments. *Geochim. Cosmochim. Acta* 52 (3), 751–765. doi: 10.1016/0016-7037(88)90335-3
- Anderson, R. F., Lehuray, A. P., Fleisher, M. Q., and Murray, J. W. (1989). Uranium deposition in saanich inlet sediments, vancouver island. *Geochim. Cosmochim. Acta* 53 (9), 2205–2213. doi: 10.1016/0016-7037(89)90344-X
- Barnes, C. E., and Cochran, J. K. (1990). Uranium removal in oceanic sediments and the oceanic U balance. *Earth Planet. Sci. Lett.* 97 (1-2), 94–101. doi: 10.1016/0012-821X(90)90101-3
- Berg, P., Risgaard-Petersen, N., and Rysgaard, S. (1998). Interpretation of measured concentration profiles in sediment pore water. *Limnol. Oceanogr.* 43 (7), 1500–1510. doi: 10.4319/lo.1998.43.7.1500
- Bigot, M., Saliot, A., Cui, X., and Li, J. (1989). Organic geochemistry of surface sediments from the huanghe estuary and adjacent bohai Sea (China). *Chem. Geol.* 75 (4), 339–350. doi: 10.1016/0009-2541(89)90006-5
- Billier, D. V., and Bruland, K. W. (2012). Analysis of Mn, Fe, Co, Ni, Cu, Zn, Cd, and Pb in seawater using the nobias-chelate PA1 resin and magnetic sector inductively coupled plasma mass spectrometry (ICP-MS). *Mar. Chem.* 130–131, 12–20. doi: 10.1016/j.marchem.2011.12.001
- Boudreau, B. P. (1997). *Diagenetic models and their implementation* (Berlin: Springer-Verlag).
- Burdige, D. J. (1993). The biogeochemistry of manganese and iron reduction in marine sediments. *Earth - Sci. Rev.* 35 (3), 249–284. doi: 10.1016/0012-8252(93)90040-E
- Canfield, D. E., and Thamdrup, B. (2009). Towards a consistent classification scheme for geochemical environments, or, why we wish the term 'suboxic' would go away. *Geobiology* 7 (4), 385–392. doi: 10.1111/j.1472-4669.2009.00214.x
- Chaillou, G., Anschutz, P., Lavaux, G., Schäfer, J., and Blanc, G. (2002). The distribution of Mo, U, and Cd in relation to major redox species in muddy sediments of the bay of Biscay. *Mar. Chem.* 80 (1), 41–59. doi: 10.1016/S0304-4203(02)00097-X
- Chen, C. C., Gong, G. C., and Shiah, F. K. (2007). Hypoxia in the East China Sea: one of the largest coastal low-oxygen areas in the world. *Mar. Environ. Res.* 64 (4), 399–408. doi: 10.1016/j.marenvres.2007.01.007
- Chi, L. B., Song, X. X., Yuan, Y. Q., Zhou, P., Cao, X. H., and Yu, Z. M. (2017). Distribution of dissolved oxygen in the yellow Sea and East China Sea in summer and winter. *Oceanol. Limnol. Sin.* 48 (6), 1337–1345. doi: 10.11693/hyhz20170500142
- Cline, J. D. (1969). Spectrophotometric determination of hydrogen sulfide in natural waters. *Limnol. Oceanogr.* 14 (3), 454–458. doi: 10.4319/lo.1969.14.3.0454
- Costa, K. M., Anderson, R. F., Mcmanus, J. F., Winckler, G., Middleton, J. L., and Langmuir, C. H. (2018). Trace element (Mn, Zn, Ni, V) and authigenic uranium (aU) geochemistry reveal sedimentary redox history on the Juan de fuca ridge, north pacific ocean. *Geochim. Cosmochim. Acta* 236 (1), 79–98. doi: 10.1016/j.gca.2018.02.016
- Dale, A. W., Meyers, S. R., Aguilera, D. R., Arndt, S., and Wallmann, K. (2012). Controls on organic carbon and molybdenum accumulation in Cretaceous marine sediments from the cenomanian-turonian interval including oceanic anoxic event 2. *Chem. Geol.* 324–325, 28–45. doi: 10.1016/j.chemgeo.2011.10.004
- Dong, T. L., Yang, G. F., and Xu, S. M. (1995). Modern sedimentary characteristics in the south of the bohai Sea. *Mar. Geol. Quaternary Geol.* 15 (4), 131–134.
- Dunk, R. M., Mills, R. A., and Jenkins, W. J. (2002). A reevaluation of the oceanic uranium budget for the Holocene. *Chem. Geol.* 190 (1-4), 45–67. doi: 10.1016/S0009-2541(02)00110-9
- Emerson, S., and Hedges, J. (2003). Sediment diagenesis and benthic flux. *Treatise Geochem.* 6, 293–319. doi: 10.1016/B0-08-043751-6/06112-0
- Emerson, S. R., and Husted, S. S. (1991). Ocean anoxia and the concentrations of molybdenum and vanadium in seawater. *Mar. Chem.* 34 (3-4), 177–196. doi: 10.1016/0304-4203(91)90002-E
- Froelich, P. N., Klinkhammer, G. P., Bender, M. L., Luedtke, N. A., Heath, G. R., Cullen, D., et al. (1979). Early oxidation of organic matter in pelagic sediments of the eastern equatorial Atlantic: suboxic diagenesis. *Geochim. Cosmochim. Acta* 43 (7), 1075–1090. doi: 10.1016/0016-7037(79)90095-4
- Gao, S., Luo, T. C., Zhang, B. R., Zhang, H. F., Han, Y. W., Zhao, Z. D., et al. (1998). Chemical composition of the continental crust as revealed by studies in East China. *Geochim. Cosmochim. Acta* 62 (11), 1959–1975. doi: 10.1016/S0016-7037(98)00121-5
- Goldberg, T., Poulton, S. W., Archer, C., Vance, D., and Thamdrup, B. (2009). Controls on Mo isotope fractionations in modern anoxic marine sediments - a key to paleoredox research. *Geochim. Cosmochim. Acta*, A445. doi: 10.1016/j.gca.2009.05.025
- Grasshoff, K., Kremling, K., and Ehrhardt, M. (1999). *Methods of seawater analysis* (Wiley-VCH, Weinheim). doi: 10.1002/9783527613984.ch4
- Gustafsson, J. P. (2003). Modelling molybdate and tungstate adsorption to ferrihydrite. *Chem. Geol.* 200 (1-2), 105–115. doi: 10.1016/S0009-2541(03)00161-X
- Helz, G. R., Miller, C. V., Charnock, J. M., Mosselmans, J. F. W., Patrick, R. A. D., Garner, C. D., et al. (1996). Mechanism of molybdenum removal from the sea and its concentration in black shales: EXAFS evidence. *Geochim. Cosmochim. Acta* 60, 3631–3642. doi: 10.1016/0016-7037(96)00195-0
- Helz, G. R., and Vorlicek, T. P. (2019). Precipitation of molybdenum from euxinic waters and the role of organic matter. *Chem. Geol.* 509, 178–193. doi: 10.1016/j.chemgeo.2019.02.001
- Herbert, L. C., Riedinger, N., Michaud, A. B., Laufer, K., Røy, H., and Jørgensen, B. B. (2020). Glacial controls on redox-sensitive trace element cycling in Arctic fjord sediments (Spitsbergen, Svalbard). *Geochim. Cosmochim. Acta* 271, 33–60. doi: 10.1016/j.gca.2019.12.005
- Hu, D. X. (1994). Some striking features of circulation in huanghai Sea and East China Sea. *Oceanol. China Seas* 1, 27–38. doi: 10.1007/978-94-011-0862-1_4
- Hu, B. Q., Li, J., Zhao, J. T., Yang, J., Bai, F. L., and Dou, Y. G. (2013). Heavy metal in surface sediments of the liaodong bay, bohai Sea: distribution, contamination, and sources. *Environ. Monit. Assess.* 185, 5071–5083. doi: 10.1007/s10661-012-2926-0
- Hyun, J. H., Kim, S. H., Mok, J. S., Cho, H., Lee, T., Vandieken, V., et al. (2017). Manganese and iron reduction dominate organic carbon oxidation in deep continental margin sediments of the ulleung basin, East Sea. *Biogeosciences* 14, 941–958. doi: 10.5194/bg-14-941-2017
- Johnson, K. S., Coale, K. H., Berelson, W. M., and Gordon, R. M. (1996). On the formation of the manganese maximum in the oxygen minimum. *Geochim. Cosmochim. Acta* 60 (8), 1291–1299. doi: 10.1016/0016-7037(96)00005-1
- Kang, X. M., Liu, S. M., and Zhang, G. L. (2014). Reduced inorganic sulfur in the sediments of the yellow Sea and East China Sea. *Acta Oceanol. Sin.* 33, 100–108. doi: 10.1007/s13131-014-0499-1

- Kim, G., Yang, H. S., and Kodama, Y. (1998). Distributions of transition elements in the surface sediments of the yellow Sea. *Cont. Shelf Res.* 18 (12), 1531–1542. doi: 10.1016/S0278-4343(98)00038-7
- Kuzyk, Z. Z., Macdonald, R. W., Stern, G. A., and Gobeil, C. (2011). Inferences about the modern organic carbon cycle from diagenesis of redox-sensitive elements in hudson bay. *J. Mar. Syst.* 88 (3), 451–462. doi: 10.1016/j.jmarsys.2010.11.001
- Kuzyk, Z. Z., Gobeil, C., Goñi, M. A., and Macdonald, R. W. (2017). Early diagenesis and trace element accumulation in north American Arctic margin sediments. *Geochim. Cosmochim. Acta* 203, 175–200. doi: 10.1016/j.gca.2016.12.015
- Li, Y. H., and Gregory, S. (1974). Diffusion of ions in sea water in deep-sea sediments. *geochim. Cosmochim. Acta* 38 (5), 703–714. doi: 10.1016/0016-7037(74)90145-8
- Li, L., Liu, Y. G., Wang, X. J., Hu, L. M., Yang, G., Wang, H. M., et al. (2020). Early diagenesis and accumulation of redox-sensitive elements in East Siberian Arctic shelves. *Mar. Geol.* 429, 10639. doi: 10.1016/j.margeo.2020.106309
- Li, L., Liu, J. H., Wang, X. J., and Shi, X. F. (2015). Dissolved trace metal distributions and Cu speciation in the southern bohai Sea. *China. Mar. Chem.* 172, 34–45. doi: 10.1016/j.marchem.2015.03.002
- Li, F. Y., and Shi, Y. L. (1995). Accumulation rates of sediment and sedimentary environment in the south bohai Sea. *J. Oceanog. Huang Hai Bohai Sea* 13 (2), 33–37.
- Li, L., Wang, X. J., Ren, Y. J., Su, H. Q., Hu, L. M., Li, Z. Q., et al. (2021). Enrichment of trace metals (V, Cu, Co, Ni, and Mo) in Arctic sediments from Siberian Arctic shelves to the basin. *J. Geophys. Res-Oceans* 126 (4), 1–14. doi: 10.1029/2020JC016960
- Lovley, D. R., Phillips, E. J. P., Gorby, Y. A., and Landa, E. R. (1991). Microbial reduction of uranium. *Nature* 350, 413–416. doi: 10.1038/350413a0
- McManus, J., Berelson, W. M., Klinkhammer, G. P., Hammond, D. E., and Holm, C. (2005). Authigenic uranium: relationship to oxygen penetration depth and organic carbon rain. *Geochim. Cosmochim. Acta* 69 (1), 95–108. doi: 10.1016/j.gca.2004.06.023
- McManus, J., Berelson, W. M., Severmann, S., Johnson, K. S., Hammond, D. E., Roy, M., et al. (2012). Benthic manganese fluxes along the Oregon-California continental shelf and slope. *Cont. Shelf Res.* 43, 71–85. doi: 10.1016/j.csr.2012.04.016
- McManus, J., Berelson, W. M., Severmann, S., Poulson, R. L., Hammond, D. E., Klinkhammer, G. P., et al. (2006). Molybdenum and uranium geochemistry in continental margin sediments: paleoproxy potential. *Geochim. Cosmochim. Acta* 70 (18), 4643–4662. doi: 10.1016/j.gca.2006.06.1564
- Morford, J., and Emerson, S. (1999). The geochemistry of redox sensitive trace metals in sediments. *Geochim. Cosmochim. Acta* 63 (11–12), 1735–1750. doi: 10.1016/S0016-7037(99)00126-X
- Morford, J. L., Emerson, S. R., Breckel, E. J., and Kim, S. H. (2005). Diagenesis of oxyanions (V, U, re, and Mo) in pore waters and sediments from a continental margin. *Geochim. Cosmochim. Acta* 69 (21), 5021–5032. doi: 10.1016/j.gca.2005.05.015
- Morford, J. L., Martin, W. R., and Carney, C. M. (2009b). Uranium diagenesis in sediments underlying bottom waters with high oxygen content. *Geochim. Cosmochim. Acta* 73 (10), 2920–2937. doi: 10.1016/j.gca.2009.02.014
- Morford, J. L., Martin, W. R., François, R., and Carney, C. M. (2009a). A model for uranium, rhenium, and molybdenum diagenesis in marine sediments based on results from coastal locations. *Geochim. Cosmochim. Acta* 73 (10), 2938–2960. doi: 10.1016/j.gca.2009.02.029
- Morford, J. L., Martin, W. R., Kalnejais, L. H., François, R., Bothner, M., and Karle, I. M. (2007). Insights on geochemical cycling of U, re and Mo from seasonal sampling in Boston harbor, Massachusetts, USA. *Geochim. Cosmochim. Acta* 71 (4), 895–917. doi: 10.1016/j.gca.2006.10.016
- Mouret, A., Anschutz, P., Lacroix, P., Chaillou, G., Hyacinthe, C., Deborde, J., et al. (2009). Benthic geochemistry of manganese in the bay of Biscay, and sediment mass accumulation rate. *Geo-Mar. Lett.* 29 (3), 133–149. doi: 10.1007/s00367-008-0130-6
- Nolting, R. F., Dalen, M., and Helder, W. (1996). Distribution of trace and major elements in sediment and pore waters of the Lena delta and laptev Sea. *Mar. Chem.* 53 (3–4), 285–299. doi: 10.1016/0304-4203(95)00095-X
- Olson, L., Quinn, K. A., Siebecker, M. G., Luther, G. W., Hastings, D., and Morford, J. L. (2017). Trace metal diagenesis in sulfidic sediments: insights from Chesapeake bay. *Chem. Geol.* 452, 47–59. doi: 10.1016/j.chemgeo.2017.01.018
- Panutrakul, S., Baeyens, M. W., and Baeyens, W. (2001). Seasonal variations in sediment sulfur cycling in the ballastplaat mudflat, Belgium. *Estuaries* 24 (2), 257–265. doi: 10.2307/1352949
- Postma, D., and Appelo, C. A. J. (2000). Reduction of Mn-oxides by ferrous iron in a flow system: column experiment and reactive transport modeling. *Geochim. Cosmochim. Acta* 64 (7), 1237–1247. doi: 10.1016/S0016-7037(99)00356-7
- Qi, J., Li, F. Y., Song, J. M., Gao, S., Wang, G. Z., and Cheng, P. (2004). Sedimentation rate and flux of the north yellow Sea. *Mar. Geol. Quaternary Geol.* 24 (2), 9–14.
- Qiao, S. Q., Shi, X. F., Zhu, A. M., Liu, Y. G., Bi, N. S., Fang, X. S., et al. (2010). Distribution and transport of suspended sediments off the yellow river (Huanghe) mouth and the nearby bohai Sea. *Estuar. Coast. Shelf S.* 86 (3), 337–344. doi: 10.1016/j.jescs.2009.07.019
- Qin, Y. W., Zheng, B. H., Lei, K., Lin, T., Hu, L. M., and Guo, Z. G. (2011). Distribution and mass inventory of polycyclic aromatic hydrocarbons in the sediments of the south bohai Sea, China. *Mar. pollut. Bull.* 62 (2), 371–376. doi: 10.1016/j.marpolbul.2010.09.028
- Qu, C. H., Chen, C. Z., Yang, J. R., Wang, L. Z., and Lu, Y. L. (1993). Geochemistry of dissolved and particulate elements in the major rivers of China (The huanghe, changjiang, and zhunjiang rivers). *Estuaries* 16 (3), 475–487. doi: 10.2307/1352595
- Roussiez, V., Ludwig, W., Probst, J. L., and Monaco, A. (2005). Background levels of heavy metals in surficial sediments of the gulf of lions (NW mediterranean): an approach based on 133Cs normalization and lead isotope measurements. *Environ. Pollut.* 138 (1), 167–177. doi: 10.1016/j.envpol.2005.02.004
- Rudick, R. L., and Gao, S. (2014). Composition of the continental crust. *Treatise Geochem.* 4, 1–51. doi: 10.1016/B978-0-08-095975-7.00301-6
- Scholz, F., Hensen, C., Noffke, A., Rohde, A., Liebetrau, V., and Wallmann, K. (2011). Early diagenesis of redox-sensitive trace metals in the Peru upwelling area - response to ENSO-related oxygen fluctuations in the water column. *Geochim. Cosmochim. Acta* 75 (22), 7257–7276. doi: 10.1016/j.gca.2011.08.007
- Shaw, T. J., Gieskes, J. M., and Jahnke, R. A. (1990). Early diagenesis in differing depositional environments: the response of transition metals in pore water. *Geochim. Cosmochim. Acta* 54 (5), 1233–1246. doi: 10.1016/0016-7037(90)90149-F
- Shi, X. F. (2014). *China Coastal seas-marine sediment* (Beijing: China ocean press).
- Shimmield, G. B., and Price, N. B. (1986). The behaviour of molybdenum and manganese during early sediment diagenesis - offshore Baja California, Mexico. *Mar. Chem.* 19 (3), 261–280. doi: 10.1016/0304-4203(86)90027-7
- Sohrin, Y., Matsui, M., and Nakayama, E. (1999). Contrasting behavior of tungsten and molybdenum in the Okinawa trough, the East China Sea and the yellow Sea. *Geochim. Cosmochim. Acta* 19–20, 63. doi: 10.1016/s0016-7037(99)00273-2
- Song, G. D., Liu, S. M., Zhang, J., Zhu, Z. Y., Zhang, G. L., Marchant, H. K., et al. (2020). Response of benthic nitrogen cycling to estuarine hypoxia. *Limnology Oceanog.* 66, 652–666. doi: 10.1002/lno.11630
- Stump, C., and Emerson, S. (2001). *Cruise report of T.G* (Seattle, WA: Thompson Cruise 131. University of Washington).
- Su, J., and Yuan, Y. (2005). *Hydrology in China coastal Sea* (Beijing: Ocean Press).
- Sundby, B., Martinez, P., and Gobeil, C. (2004). Comparative geochemistry of cadmium, rhenium, uranium, and molybdenum in continental margin sediments. *Geochim. Cosmochim. Acta* 68 (11), 2485–2493. doi: 10.1016/j.gca.2003.08.011
- Tribouillard, N., Riboulleau, A., Lyons, T., and Baudin, F. (2004). Enhanced trapping of molybdenum by sulfurized organic matter of marine origin in mesozoic limestones and shales. *Chem. Geol.* 213, 385–401. doi: 10.1016/j.chemgeo.2004.08.011
- Tromp, T., van Cappellen, P., and Key, R. (1995). A global model for the early diagenesis of organic carbon and organic phosphorus in marine sediments. *Geochim. Cosmochim. Acta* 59, 1259–1284. doi: 10.1016/0016-7037(95)00042-x
- van de Velde, S. J., Hidalgo-Martinez, S., Callebaut, I., Antler, G., James, R. K., Leermakers, M., et al. (2020). Burrowing fauna mediate alternative stable states in the redox cycling of salt marsh sediments. *Geochim. Cosmochim. Acta* 276, 31–49. doi: 10.1016/j.gca.2020.02.021
- Volz, J. B., Liu, B., Koster, M., Henkel, S., Koschinsky, A., and Kasten, S. (2020). Post-depositional manganese mobilization during the last glacial period in sediments of the eastern clarion-clipperton zone, pacific ocean. *Earth Planet. Sci. Lett.* 532, 116012. doi: 10.1016/j.epsl.2019.116012
- Vorlicek, T. P., Kahn, M. D., Kasuya, Y., and Helz, G. R. (2004). Capture of molybdenum in pyrite-forming sediments: role of ligand-induced reduction by polysulfides. *Geochim. Cosmochim. Acta* 68, 547–556. doi: 10.1016/S0016-7037(03)00444-7
- Wang, B. D. (1997). Formation mechanism of maximum value in vertical distribution of dissolved oxygen in the yellow Sea. *J. Oceanog. Huanghai Bohai Seas* 15 (3), 10–15.
- Wang, B. D. (2009). Hydromorphological mechanisms leading to hypoxia off the changjiang estuary. *Mar. Environ. Res.* 67 (1), 53–58. doi: 10.1016/j.marenvres.2008.11.001
- Wang, X. J., Li, L., Liu, J. H., Wu, Y. H., Gao, J. J., Cao, P., et al. (2019). Early diagenesis of redox-sensitive trace metals in the northern Okinawa trough. *Acta Oceanol. Sin.* 38 (12), 14–25. doi: 10.1007/s13131-019-1512-5
- Wang, D. L., and Wilhelmy, S. A. S. (2009). Vanadium speciation and cycling in coastal waters. *Mar. Chem.* 117 (1–4), 52–58. doi: 10.1016/j.marchem.2009.06.001
- Wang, H. J., Yang, Z. S., Saito, Y., Liu, J. P., Sun, X. X., and Wang, Y. (2007). Stepwise decreases of the huanghe (Yellow river) sediment load, (1950–2005): impacts of climate change and human activities. *Global Planet. Change* 57 (3–4), 331–354. doi: 10.1016/j.gloplacha.2007.01.003
- Wang, L. S., Zhang, C. S., Wang, H., and Shi, X. Y. (2015). Horizontal distribution features of biogenic elements in bohai Sea and the yellow Sea in summer. *Mar. Environ. Sci.* 34 (3), 361–366. doi: 10.13634/j.cnki.mes.20150307
- Wanty, R. B., and Goldhaber, M. B. (1992). Thermodynamics and kinetics of reactions involving vanadium in natural systems: accumulation of vanadium in sedimentary rocks. *Geochim. Cosmochim. Acta* 56, 1471–1483. doi: 10.1016/0016-7037(92)90217-7
- Wehrli, B., and Stumm, W. (1989). Vanadyl in natural waters: adsorption and hydrolysis promote oxygenation. *Geochim. Cosmochim. Acta* 53 (1), 69–77. doi: 10.1016/0016-7037(89)90273-1
- Wei, Q. S., Wang, B. D., Yao, Q. Z., Xue, L., Sun, J. C., Xin, M., et al. (2019). Spatiotemporal variations in the summer hypoxia in the bohai Sea (China) and

- controlling mechanisms. *Mar. Pollut. Bull.* 138, 125–134. doi: 10.1016/j.marpolbul.2018.11.041
- Whitmore, L. M., Morton, P. L., Twining, B. S., and Shiller, A. M. (2019). Vanadium cycling in the Western Arctic ocean is influenced by shelf-basin connectivity. *Mar. Chem.* 216, 103701. doi: 10.1016/j.marchem.2019.103701
- Wu, Y. J., Fan, D. D., Wang, D. L., and Yin, P. (2020). Increasing hypoxia in the changjiang estuary during the last three decades deciphered from sedimentary redox-sensitive elements. *Mar. Geol.* 419, 106044. doi: 10.1016/j.margeo.2019.106044
- Xia, X. M., Yang, H., Li, Y., Li, B. G., and Pan, S. M. (2004). Modern sedimentation rates in the contiguous Sea area of changjiang estuary and hangzhou bay. *Acta Sedimentol. Sin.* 22 (1), 130–135.
- Xu, S. M. (2007). Distribution and environment significance of redox sensitive trace elements of the changjiang estuary hypoxia zone and its contiguous Sea area. *Acta Sedimentol. Sin.* 25 (5), 759–766. doi: 10.2514/1.26230
- Xu, L. L., Wu, D. X., Lin, X. P., and Ma, C. (2009). The study of the yellow Sea warm current and its seasonal variability. *J. Hydrodynam. Ser. B* 21 (2), 159–165. doi: 10.1016/S1001-6058(08)60133-X
- Yamada, M., Wang, Z. L., and Kato, Y. (2006). Precipitation of authigenic uranium in suboxic continental margin sediments from the Okinawa Trough. *Estuar. Coast. Shelf S.* 66 (3–4), 570–579. doi: 10.1016/j.ecss.2005.11.002
- Yang, S. Y., Jung, H. S., Lim, D., and Li, C. X. (2003). A review on the provenance discrimination of sediments in the yellow Sea. *Earth Sci. Rev.* 63 (1–2), 93–120. doi: 10.1016/S0012-8252(03)00033-3
- Yang, S. L., Liu, G. X., Du, R. Z., and Zhang, B. (1993). Study on the modern sedimentation rate through ²¹⁰Pb age dating, liaodong bay. *Acta Sedimentol. Sin.* 11 (1), 128–135.
- Yuan, H. M., Song, J. M., Li, X. G., Li, N., and Duan, L. Q. (2012). Distribution and contamination of heavy metals in surface sediments of the south yellow Sea. *Mar. Pollut. Bull.* 64 (10), 2151–2159. doi: 10.1016/j.marpolbul.2012.07.040
- Zhang, R., Pan, S. M., Wang, Y. P., and Gao, J. H. (2009). Sedimentation rates and characteristics of radionuclide ²¹⁰Pb at the subaqueous delta in changjiang estuary. *Acta Sedimentol. Sin.* 27 (4), 704–713.
- Zhang, L. J., Wang, L., Cai, W. J., Liu, D. M., and Yu, Z. G. (2013). Impact of human activities on organic carbon transport in the yellow river. *Biogeosciences* 10, 2513–2524. doi: 10.5194/bg-10-2513-20
- Zhang, S. W., Wang, Q. Y., Lü, Y., Cui, H., and Yuan, Y. L. (2008). Observation of the seasonal evolution of the yellow Sea cold water mass in 1996–1998. *Cont. Shelf Res.* 28 (3), 442–457. doi: 10.1016/j.csr.2007.10.002
- Zhao, H. D., Kao, S. J., Zhai, W. D., Zang, K. P., Zheng, N., Xu, X. M., et al. (2017). Effects of stratification, organic matter remineralization and bathymetry on summertime oxygen distribution in the bohai Sea, China. *Cont. Shelf Res.* 134, 15–25. doi: 10.1016/j.csr.2016.12.004
- Zhao, B., Yao, P., Bianchi, T. S., and Yu, Z. G. (2021). Controls on organic carbon burial in the Eastern China marginal seas: a regional synthesis. *Global Biogeochem. Cy.* 35 (4), 1–27. doi: 10.1029/2020GB006608
- Zheng, Y., Anderson, R. F., Geen, A. V., and Fleisher, M. Q. (2002). Remobilization of authigenic uranium in marine sediments by bioturbation. *Geochim. Cosmochim. Acta* 66 (10), 1759–1772. doi: 10.1016/S0016-7037(01)00886-9
- Zheng, Y., Anderson, R. F., Geen, A. V., and Kuwabara, J. (2000). Authigenic molybdenum formation in marine sediments: a link to pore water sulfide in the Santa Barbara basin. *Geochim. Cosmochim. Acta* 64 (24), 4165–4178. doi: 10.1016/S0016-7037(00)00495-6
- Zhu, Z. Y., Zhang, J., Wu, Y., Zhang, Y. Y., Lin, J., and Liu, S. M. (2011). Hypoxia off the changjiang (Yangtze river) estuary: oxygen depletion and organic matter decomposition. *Mar. Chem.* 125 (1–4), 108–116. doi: 10.1016/j.marchem.2011.03.005
- Zou, J. J., Shi, X. F., Li, N. S., Liu, J. H., and Zhu, A. M. (2010). Early diagenetic processes of redox sensitive elements in Yangtze estuary. *Earth Sci. - J. China Univ. Geosci.* 35 (1), 31–42. doi: 10.3799/dqkx.2010.004